ADVANCED FUNCTIONAL MATERIALS
www.afm-journal.de

Cell-Delivering Injectable Hydrogels with Tunable Microporous Structures Improve Therapeutic Efficacy for Volumetric Muscle Loss

*Hana Yasue, Tetsushi Taguchi, Taka-Aki Asoh, and Akihiro Nishiguchi**

Volumetric muscle loss (VML) is a traumatic or surgical injury to the skeletal muscles that causes irrecoverable functional loss, leading to chronic deficits and long-term disability. Although cell transplantation is a potent therapeutic approach, treating VML remains challenging because of the poor graft survival of cell suspensions injected into defects. Here, the development of tunable micropore-forming injectable hydrogels is reported to deliver mesenchymal stem cells (MSCs) for VML treatment. The molecular modification of gelatin with hydrogen-bonding functional groups induces liquid–liquid phase separation when mixed with chemically crosslinkable gelatin to form injectable hydrogels with tunable microporous structures. MSCs encapsulated in porous hydrogels show higher cell adhesion, spreading, proliferation, and secretion of paracrine signals than those encapsulated in non-porous hydrogels. Porous hydrogels enhance cell infiltration and myoblast differentiation. Additionally, porous hydrogels improve the graft survival of transplanted MSCs in VML mouse models and ameliorate therapeutic efficiency. This controlled microstructure-containing injectable hydrogel may serve as a cell-delivering scaffold to improve the efficacy of cell transplantation therapies in regenerative medicine.

1. Introduction

Skeletal muscle has a high tissue regenerative capacity after traumatic damage.[1] However, severe damage resulting in >15% loss of muscle mass due to car accidents, sports injuries, or battlefield injuries hinders the inherent muscle regeneration process and does not heal without therapeutic intervention.[2–5] Such traumatic or surgical loss of skeletal muscles is defined as volumetric muscle loss (VML), which impairs muscle strength and contractility.[6] VML causes chronic deficits and long-term disabilities that affect health, mobility, and quality of life.[7–9] The current standard treatment for VML involves the transfer of muscle flaps and other surgical interventions; however, these methods are highly invasive and result in undesirable aesthetic and functional outcomes.[10–12] To overcome these limitations, regenerative medicine has emerged as an attractive option for muscle tissue regeneration. Regenerative medicine aims to heal tissues, both structurally and functionally, by transplanting patient-derived cells. In particular, cell transplantation using mesenchymal stem cells (MSCs) has been highlighted because of their growth factor-secreting functions,[13] multipotency,[14] and immunomodulatory abilities.[15] Despite the high therapeutic ability of MSCs and their potential treatment against VML, injecting a cell suspension into the defects often results in poor graft survival, which remains a barrier to clinical translation.[16]

Injectable hydrogels can be used as cell-delivering carriers to promote the engraftment and therapeutic efficiency of cell transplantation. Injectable hydrogels are catheter- or syringe-deliverable biomaterials that form hydrogels through liquid-to-solid transitions. Injectable hydrogels protect cells from mechanical stress during injection and support the transplanted cells as scaffolds at defect sites.[17] In particular, gelatin-based injectable hydrogels have been widely used in numerous studies owing to their biocompatibility, biodegradability, and ability to support cell functions such as cell growth, differentiation, and tissue regeneration.[18–19] Injectable hydrogel-based cell delivery approaches for muscle tissue regeneration have also been developed.[20–21] However, injectable hydrogels often possess densely crosslinked polymer networks without micro-sized pores, resulting in limited nutrient/gas exchange, proliferation, poor integration with host tissues, and delayed muscle

H. Yasue, T. Taguchi, T.-A. Asoh, A. Nishiguchi
Graduate School of Advanced Engineering
Tokyo University of Science
6-3-1 Niijuku, Katsushika-ku, Tokyo 125–8585, Japan
E-mail: NISHIGUCHI.Akihiro@nims.go.jp
H. Yasue, T. Taguchi, A. Nishiguchi
Biomaterials Field
Research Center for Macromolecules and Biomaterials
National Institute for Materials Science
1-1 Namiki, Tsukuba, Ibaraki 305-0044, Japan

The ORCID identification number(s) for the author(s) of this article can be found under https://doi.org/10.1002/adfm.202508278

DOI: 10.1002/adfm.202508278

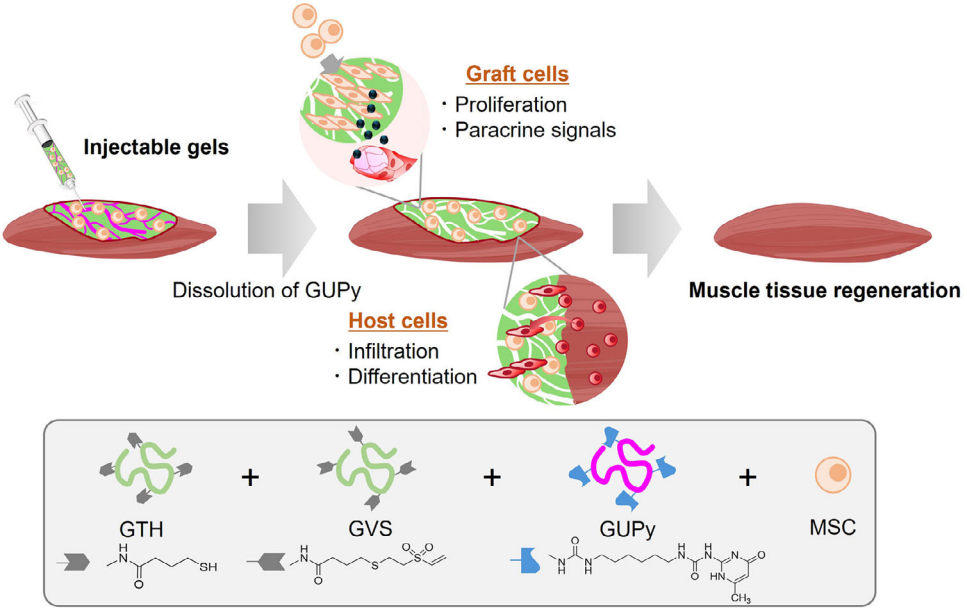

Figure 1. Schematic image of the treatment of volumetric muscle loss (VML) using porous hydrogel. Mesenchymal stem cells (MSCs) encapsulated in porous hydrogels were transplanted into VML defects. Thiol group-modified gelatin (GTH), vinyl sulfone group-modified gelatin (GVS), and UPy-modified gelatin (GUPy) formed hydrogels, and GUPy was dissolved after transplantation to form interconnected microporous structures. The micropores worked as a scaffold and promoted the proliferation and secretion of paracrine signals of graft cells and induced the infiltration and differentiation of host cells.

tissue regeneration.[22–24] Although there are several approaches for creating porous scaffolds, including electrospinning,[25–27] freeze-drying,[28–29] and biofabrication,[30] these are not injectable and have drawbacks, such as invasiveness for transplantation, poor operability, and low tissue adhesion. To balance both injectability and porosity, several strategies, including the use of porogens,[31–32] granular gels,[33] and peptide nanofibers,[34] have been reported; however, these approaches often lack interconnected micropores for cell-cell interactions, mechanical strength of gels, and tunability of microstructures.

In this study, we developed injectable hydrogels with tunable microporous structures for stem cell transplantation to treat VML (**Figure 1**). The molecular modification of gelatin with hydrogen-bonding functional groups, 2-ureido-4[^{1}H]-pyrimidinone (UPy) units, induces liquid–liquid phase separation (LLPS) when mixed with UPy-unmodified, chemically crosslinkable gelatin to form porous injectable hydrogels with microcapillary network-like pores.[35–36] The microstructures in the hydrogels were controlled by LLPS, and the chemical crosslinking and dissolution of UPy-modified gelatin (GUPy) provided microporous hydrogels. Porous hydrogels with controlled internal structures promote donor cell spreading, proliferation, and secretion of signaling molecules, which are essential for muscle tissue regeneration. Moreover, porous structures enhance the cellular infiltration and differentiation of myoblasts, which may lead to their rapid integration into host tissues. In VML mouse models, the porous injectable hydrogels improved graft survival and therapeutic efficacy against muscle tissue defects. These findings demonstrate that this injectable hydrogel with interconnected microporous structures has immense potential as a cell-delivery carrier for regenerating injured muscle tissues.

2. Results and Discussion

2.1. Structural and Mechanical Properties of Hydrogels

Porous hydrogels were engineered in two steps. First, the LLPS hydrogels were formed by mixing Thiol group-modified gelatin (GTH), vinyl sulfone group-modified gelatin (GVS), and GUPy. GUPy induced LLPS formation via hydrogen-bonding-driven self-association, and GTH and GVS were chemically cross-linked via Michael addition to form a hydrogel with an LLPS structure (**Figure 2a**). Second, GUPy was dissolved after injection into a physiological environment to obtain microporous structures. The microstructures inside the hydrogels can be tuned by controlling the LLPS behavior of gelatin. The introduction of UPy units into the gelatin was confirmed by ^{1}H NMR spectroscopy (Figure S1, Supporting Information). Confocal laser scanning microscopy (CLSM) observations showed that the hydrogel composed of GTH, GVS, and GUPy (porous hydrogel) had micrometer-sized capillary-like LLPS structures, whereas there were no microporous structures in the hydrogel composed of GTH, GVS, or phosphate-buffered saline (PBS) (nonporous hydrogel) (Figure 2b). This result suggests that GUPy with hydrogen-bonded moieties induces LLPS by functioning as a self-assembling patch, enabling the fabrication of microporous hydrogels. Furthermore, the internal structure of the porous hydrogels was analyzed using 3D analysis software. The 3D-reconstructed images showed that the porous hydrogels possessed interconnected 3D pores within the hydrogels (Figure 2c; Movie S1, Supporting Information). Rheological measurements revealed that after mixing the pre-solution of GTH, GVS, and GUPy, the porous hydrogels turned from liquid to gel within a few minutes, and the storage modulus (G') reached a plateau at

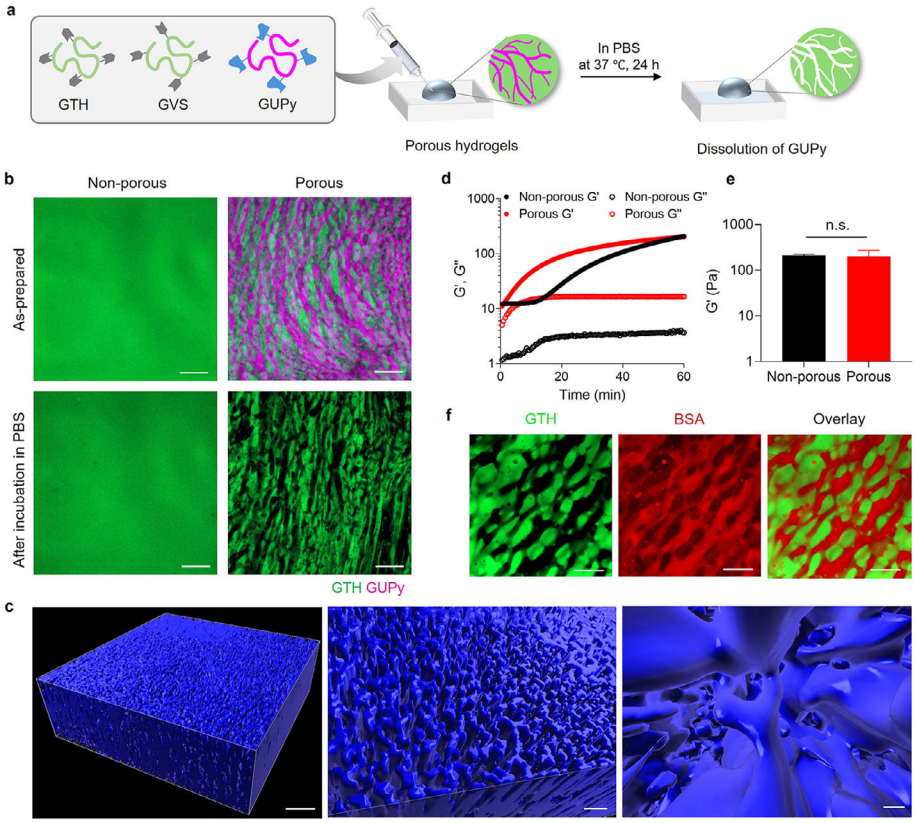

Figure 2. Characterization of LLPS hydrogels. a) Schematic illustration of the preparation of porous hydrogels. Mixing chemically crosslinkable gelatin with GUPy induced LLPS. LLPS hydrogels formed microporous structures in situ after the injection. b) CLSM images of hydrogels of non-porous (GTH+GVS) and porous hydrogels (GTH+GVS+GUPy). GTH-fluorescein (green) and GUPy-Cy5 (violet) were used for the visualization. c) 3D-reconstructed internal structures of porous hydrogels. Higher magnification of images was shown on the right. d) Rheological measurement of non-porous and porous hydrogels. e) Shear storage modulus of hydrogels. The measurements were repeated using different samples ($n = 3$). f) Diffusion test of BSA into porous hydrogels. Rhodamine-labeled BSA was added to porous hydrogels of GTH-fluorescein (green). Data was analyzed by the two-tailed Student's *t*-test. n.s. denotes not significant. Scale bars represent 50 µm for (b, c-left) and 20 µm for (c-middle, f), and 2 µm for (c-right).

≈200 Pa after 1 h (Figure 2d). The G' of non-porous and porous hydrogels were almost the same (Figure 2e). The swelling ratios of the non-porous and porous hydrogels in PBS were 15.3 and 17.5%, respectively (Figure S2, Supporting Information). Additionally, the non-porous and porous hydrogels were degraded by collagenase within a day, indicating their biodegradability. (Figure S3, Supporting Information).

To investigate the effect of the internal microporous structures of the hydrogels on mass transport, protein diffusion was evaluated using rhodamine-labeled bovine serum albumin (BSA) by CLSM imaging. CLSM observations showed that the porous hydrogels promoted BSA diffusion into the voids formed by the dissolution of GUPy during incubation (Figure 2f). This result indicates that the interconnected micropores in hydrogels may play an important role in supplying nutrients and oxygen to encapsulated cells to maintain cellular functions such as survival, which mimics blood capillary networks.

2.2. Cellular Behavior in Microporous Hydrogels

Three LLPS-induced hydrogels with different pore sizes were prepared to verify the effect of the microporous structure on the cell morphology. The pore size was tuned by varying the GUPy concentration and using various biopolymers such as hyaluronic acid sodium salt (HA). CLSM observations showed that LLPS was formed in all three hydrogels, and microsized pores were produced after incubation in PBS (**Figure 3a**). Pore size of porous hydrogels can be tuned in the range of 8–22 µm, while no micropores were observed in non-porous hydrogel (Figure 3b). Porous hydrogels with different micropore sizes were defined as small micropores (GTH [10 wt.%], GVS [10 wt.%], and GUPy [15 wt.%], volume ratio 1:1:2), medium micropores (thiol group-modified GUPy [GUPyTH] [10 wt.%], vinyl sulfone group-modified GUPy [GUPyVS] [10 wt.%], and HA [2 wt.%], volume ratio 1:1:1), and large micropores (GTH [10 wt.%], GVS [10 wt.%], and GUPy [10 wt.%], volume ratio 1:1:2), respectively. Regarding hydrogel with medium micropores, HA was mixed with GUPyTH and GUPyVS instead of gelatin to produce uniform microfibrous structures.[35] The intermolecular interactions between gelatin and the sequential LLPS behavior can be tailored by the UPy units; therefore, this method can be used to control the internal microgeometry of hydrogels. However, the overall porosities were comparable among the hydrogels because the volume fraction of porogens (GUPy and HA) in each hydrogel was almost the same (Figure S4, Supporting Information).

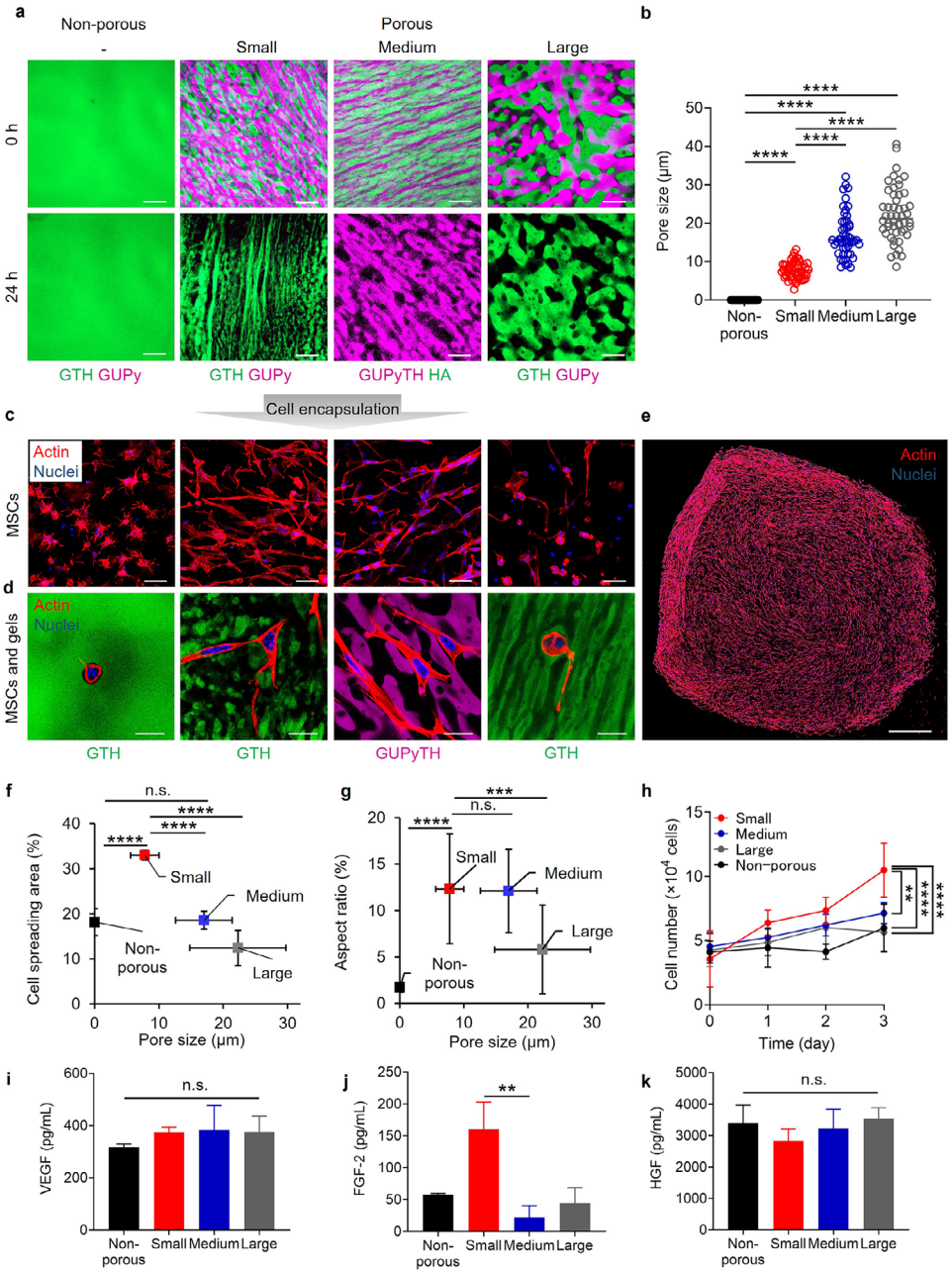

Figure 3. Porous hydrogels enhanced cell adhesion and spreading. a) CLSM images of non-porous and porous hydrogels with small, medium, and large micropores. GTH-fluorescein, GUPy-Cy5, GUPyTH-Cy5, and HA-fluorescein were used for the visualization. Hydrogels were immersed in PBS for 24 h. b) Pore size of non-porous and porous hydrogels. The 50 points were counted from CLSM images obtained from three replicates. c,d) Low (top) and high (bottom) magnification of CLSM images of MSCs encapsulated in non-porous and porous hydrogels. GTH-fluorescein (green), GUPyTH-Cy5, phalloidin (red), and DAPI (blue) were used for the visualization. e) Gross images of MSCs encapsulated in porous hydrogels. Cells were cultured for 2 days. f,g) Cell area and aspect ratio of MSCs in hydrogels ($n = 3$). h) Proliferation of MSCs encapsulated in non-porous and porous hydrogels ($n = 4$). i–k) Quantification of VEGF, FGF-2, and HGF secretion from MSCs encapsulated in non-porous and porous hydrogels ($n = 4$). $^{**}p < 0.01$, $^{****}p < 0.0001$ analyzed by the one-way (f,k) and the two-way (h) analysis of variance (ANOVA) with Tukey's multiple comparison *post hoc* test. $^{***}p < 0.001$, $^{****}p < 0.0001$ analyzed by Kruskal–Wallis followed by Dunn's multiple comparison test (b,g,i,j). n.s. denotes not significant. Scale bars represent 50 μm for (a), (c), 20 μm for (d), and 1 mm for (e).

Mouse MSCs were encapsulated in hydrogels with different micropore sizes, and their cellular behavior was observed using CLSM. To improve the therapeutic efficacy of MSCs transplantation, the effect of hydrogel pore size on cell function must be understood. CLSM observations demonstrated that most of the cells in non-porous hydrogels adhered to the hydrogels but were not elongated, whereas hydrogels with LLPS structures formed micropores during culture without a washing step, and cells in porous hydrogels showed higher cell spreading (Figure 3c). In addition, observation of the localization of cells and the gel matrix showed that cells in non-porous hydrogels were restricted from spreading by the chemically crosslinked gelatin scaffolds, whereas cells in porous hydrogels elongated along the pores formed by the dissolution of GUPy or HA (Figure 3d). Microporous hydrogels achieve rapid cell spreading in short-term cultures without enzymatic matrix degradation. Among porous hydrogels, small micropores (8 μm) facilitated substantial cell spreading throughout the hydrogel (Figure 3e). To quantify cell morphology, the cell adhesion area and aspect ratio were measured. Hydrogels with smaller micropores exhibited the largest cell adhesion areas among the non-porous, medium, and large micropore hydrogels. Cell spreading was not directly proportional to pore size but peaked at an optimal pore size (Figure 3f). Moreover, small micropores induced higher cell elongation than non-porous and large micropores (Figure 3g). These results indicate that the pore size has a significant impact on cell adhesion, which is in good agreement with a previous report.[37]

In addition, cell-delivering injectable hydrogels must closely communicate with encapsulated donor cells and host cells surrounding the defects to improve graft cell survival. To explore the effect of the microporous structures of the hydrogels on MSCs, MSCs were encapsulated in each type of hydrogel, and the proliferation and secretion of cytokines were evaluated. The number of cells in the hydrogel with small micropores showed the largest increase compared to that in the non-porous and other porous hydrogels, indicating that small microporous structures enhanced cell proliferation (Figure 3h). Regarding the paracrine signaling of growth factors, MSCs are known to produce many bioactive molecules related to the healing process of injured skeletal muscles, such as insulin-like growth factor (IGF), transforming growth factor-β (TGF-β), VEGF, FGF-2, and HGF.[5,38] Especially, vascular endothelial growth factor (VEGF), fibroblast growth factor-2 (FGF-2), and hepatocyte growth factor (HGF) are crucial for muscle regeneration because of their angiogenic and proliferative properties.[5,39–41] The secretion of cytokine, VEGF, and HGF, from MSCs encapsulated in each hydrogel, was quantified using ELISA (Figure 3i–k). Importantly, FGF-2 from MSCs increased when cells were cultured in a hydrogel with small micropores compared to other hydrogels (Figure 3j). Moreover, the amount of secreted FGF-2 per cell was 25.2 pg $mL^{-1}/10^4$ cells in the small porous hydrogel, which was the highest among the hydrogels. This suggests that porous hydrogels with small micropores upregulate the FGF-2 secretory ability of MSCs (Figure S5b, Supporting Information). In contrast, the amount of VEGF and HGF secreted per cell in small micropores was comparable to that in other hydrogels, including non-porous hydrogels, partially because the hypoxic conditions in non-porous hydrogels may upregulate VEGF and HGF expression in MSCs (Figure S5a,c, Supporting Information).[42] This method of tuning the internal structure of hydrogels using LLPS enabled the formation of hydrogels with various pore sizes. Hydrogels with small micropores enhanced cellular adhesion, spreading, proliferation, and secretion of FGF-2. Therefore, porous hydrogels with small micropores were used in subsequent experiments.

2.3. The Effect of Microporous Structures on MSCs and Myoblasts

To regenerate skeletal muscle tissue, the scaffold must allow cell infiltration, alignment, and fusion to form a functional muscle construct.[22,43] For this reason, it is important to design hydrogel environments that support cell infiltration from host tissues and their differentiation on defect sites. To address the effects of microporous structures on host cells, mouse myoblasts (C2C12) were used as a model. C2C12 cells were seeded onto the hydrogel and cultured for 4 days to evaluate their infiltration into the hydrogels. CLSM observations showed that the porous hydrogels induced faster infiltration of myoblasts than the non-porous hydrogels in the cell invasion assay (**Figure** 4a). This result indicated that the microporous structure facilitated cell infiltration from the interface with the host tissues, which led to rapid integration of the hydrogels into the host. Myoblast differentiation was evaluated by myosin heavy chain (MHC) staining as a marker of skeletal muscle differentiation and maturation. Myoblasts encapsulated in porous hydrogels exhibited intense MHC fluorescence and fused to form myotubes, whereas fused cells were not observed in non-porous hydrogels (Figure 4b). The myotubes cultured in porous hydrogels were significantly longer than those cultured in non-porous hydrogels and were almost the same as those cultured in 2D culture. These results suggest that the interconnected micropores function as voids for cell infiltration and enhance the differentiation and fusion of myoblasts toward muscle tissue maturation, thereby contributing to the regeneration of functional skeletal muscle tissues.

2.4. Graft survival of MSCs in VML Model

Hydrogel biodegradability was evaluated prior to cell transplantation. Optimal biomaterials should support cell survival and proliferation and exhibit optimum biodegradation rates compatible with myogenesis. Gelatin is a naturally occurring polymer with excellent biocompatibility and biodegradability. Gelatin-based chemically crosslinked hydrogels may possess sufficient mechanical strength and a controlled biodegradation rate. To evaluate their biodegradability, the hydrogels were subcutaneously implanted into mice. Histological observations showed that the porous hydrogels were mostly degraded 28 days after implantation (Figure S6, Supporting Information). Many cells (e.g., neutrophils and macrophages) infiltrated the host tissue into the hydrogels through the porous structures, suggesting that porous structures may promote the integration of hydrogels into the host.

VML therapy remains a challenge in regenerative medicine because of the poor graft survival of cell suspensions injected into the body. To address whether porous hydrogels improve cell engraftment in VML, MSCs encapsulated in hydrogels

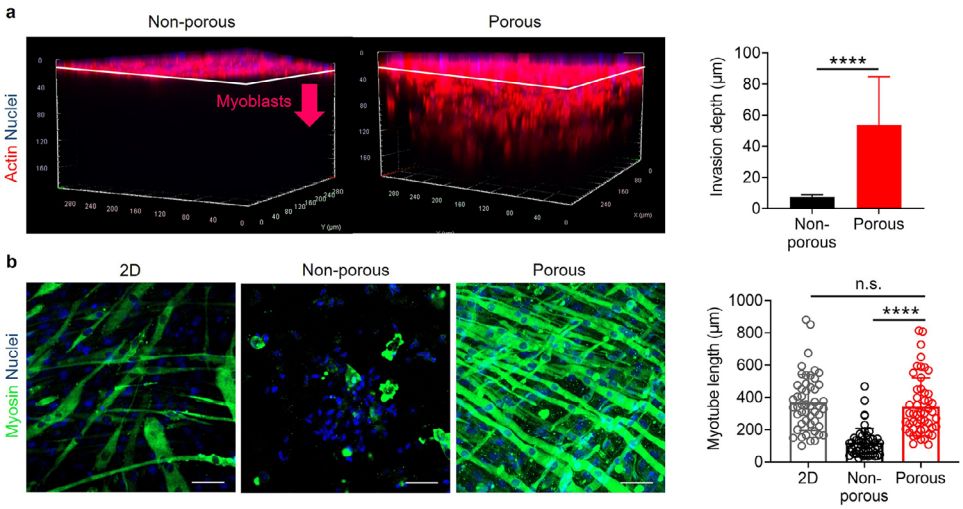

Figure 4. Effects of microporous structures of hydrogels on the functions of MSCs and myoblasts. a) CLSM images of the infiltration of myoblasts seeded onto hydrogels. The depth of cells was quantified using 3D-analysis software ($n = 3$). b) CLSM images of myoblast differentiation cultured on 2D and in hydrogels. Myotube length was quantified using ImageJ ($n = 50$). $^{****}p < 0.0001$ analyzed by the Mann–Whitney U test (a) and Kruskal–Wallis followed by Dunn's multiple comparison test (b). n.s. denotes not significant. Scale bars represent 50 μm.

were transplanted into a VML mouse model. The VML mouse model was established by cutting the tibialis anterior (TA) muscles (**Figure** 5a). DiI-stained MSCs were suspended in PBS, encapsulated in non-porous or porous hydrogels, and injected into the defect. One week after transplantation, graft survival was analyzed using CLSM. Although the fluorescence intensity of MSCs transplanted with a cell suspension (MSCs alone) or non-porous hydrogels was unevenly distributed within the defects, MSCs delivered via the porous hydrogels remained localized at the injection sites (Figure 5b). The area of MSCs in the porous hydrogels was significantly larger than that in the cell suspensions (Figure 5c). This result suggests that microporous structures support cell graft survival by providing an adhesion scaffold for MSCs, whereas densely crosslinked polymer networks in non-porous hydrogels hinder their integration with host tissues.

2.5. Muscle Tissue Regeneration by MSC Delivery Using Porous Hydrogels

Despite numerous studies on muscle tissue regeneration using MSCs, owing to their secretory functions, their therapeutic efficiency remains a challenge because of poor graft survival.[16] To address the therapeutic efficiency of the porous structures, MSCs were transplanted into the VML defects using hydrogels (**Figure** 6a). The weight of the TA muscles 4 weeks after the transplantation of MSCs with porous hydrogels was 1.4 times higher than that of the defect group, 1.3 times higher than that of non-porous hydrogels, and comparable to that of the sham group (without muscle defects) (Figure 6b). From the hematoxylin and eosin (HE)- and Masson's trichrome (MT)-stained cross-sectional images, the TA muscle treated with porous hydrogels showed 1.6 and 1.4 times fold increases in muscle tissue area compared to the defect groups and non-porous hydrogels, respectively, and was comparable to that of the sham group (Figure 6c–e). Cross-sectional images stained with MT showed that the reconstructed tissues within the porous hydrogels were composed of muscle fibers, whereas muscle defects treated with cell suspensions or non-porous hydrogels lacked tissue formation even four weeks after treatment. Wound healing is a dynamic process that overlaps in time and space and involves activation of the blood coagulation cascade and inflammatory pathways (inflammation), cell infiltration and angiogenesis (tissue formation), maturation, and matrix degradation (tissue remodeling).[44] Micropores in injectable hydrogels may serve as an adhesive matrix to induce cell infiltration and accelerate wound healing. Although several studies have been conducted on muscle tissue regeneration using porous scaffolds, muscle tissue regeneration has only been achieved using cell-delivered injectable hydrogels with LLPS-induced tunable microporous structures. This method allows for the creation of interconnected microporous structures and improves the survival of transplanted MSCs and therapeutic efficacy against VML by enhancing cell-material interactions.

3. Conclusion

In this study, injectable hydrogels with tunable microporous structures were developed to deliver MSCs for the treatment of VML. Porous hydrogels with a pore size of ≈8 μm significantly promoted the spreading, proliferation, and cytokine secretion of MSCs. Interconnected micropores with appropriate pore sizes improve the functions of MSCs by providing an adhesion scaffold and supplying oxygen and nutrients to the encapsulated cells. Furthermore, the porous structures supported cell infiltration and myoblast differentiation, indicating that micropores may rapidly integrate into host tissues. Notably, porous hydrogels improved cell engraftment in the VML mouse model, and MSCs contributed to muscle tissue regeneration. These results suggest that stem cell transplantation using porous hydrogels enables active communication with host tissues post-transplantation, resulting in an improved therapeutic efficiency

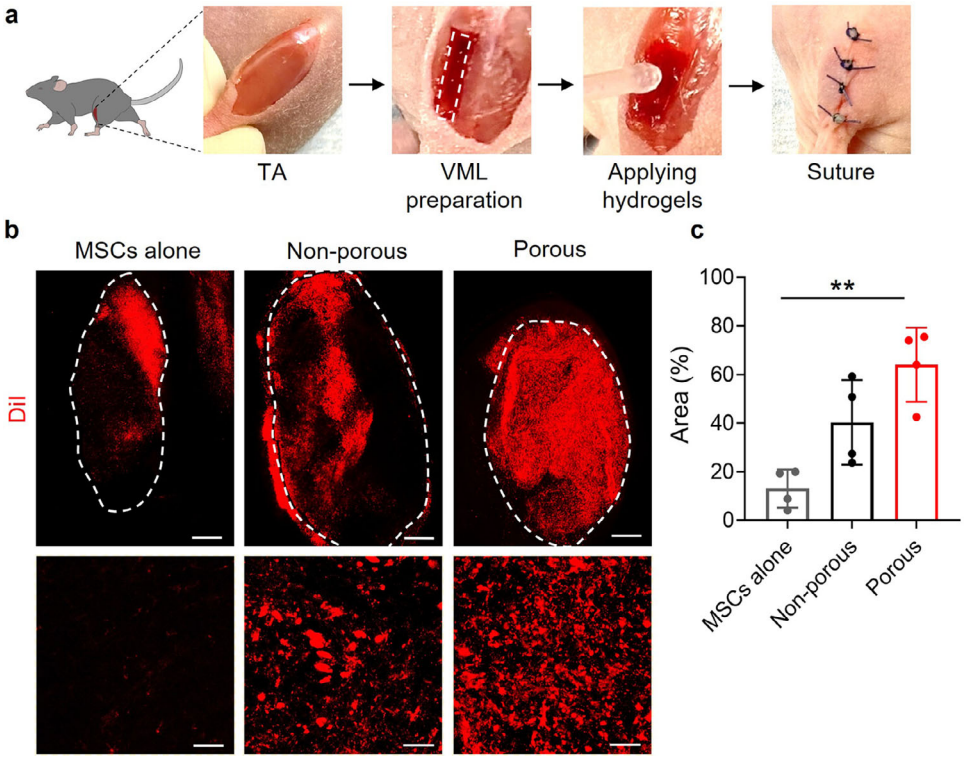

Figure 5. Graft survival of transplanted MSCs using the mouse VML model. a) DiI-stained MSCs suspended in PBS (MSCs alone) or encapsulated in non-porous and porous hydrogel were transplanted to TA muscle defects. b) CLSM images of transplanted MSCs ($n = 4$). MSCs were stained with DiI before the injection. On day 7 after the transplantation, tissues were collected and observed by CLSM. c) Area of transplanted MSCs ($n = 4$). $^{**}p < 0.01$ analyzed by the one-way ANOVA with Tukey's multiple comparison post hoc test (c). Scale bars represent 1 mm (top) and 50 µm (bottom) for (b).

for VML. The limitation of this injectable hydrogel is its operability during injection, as more than two solutions must be mixed using a spray device. Therefore, the development of single-syringe-type injectable hydrogels for cell delivery remains challenging. This injectable hydrogel with a tunable microstructure could serve as a scaffold to improve the therapeutic efficacy of cell transplantation.

4. Experimental Section

Materials: The 1,6-diisocyanatohexane, 2,4,6-trinitrobenzenesulfonic acid sodium salt dihydrate (TNBS), and divinyl sulfone were purchased from Tokyo Chemical Industry Co., Ltd. (Tokyo, Japan). Tris(2-carboxyethyl)phosphine hydrochloride (TCEP-HCl), collagenase, and PBS were purchased from Nacalai Tesque Inc. (Kyoto, Japan). Porcine skin-derived gelatin, 2-amino-4-hydroxy-6-methylpyrimidine, γ-thiobutyrolactone, 5,5′-dithiobis(2-nitrobenzoic acid) (DTNB), fluorescein isothiocyanate (FITC), RPMI1640 medium, and fetal bovine serum (FBS) were purchased from Sigma-Aldrich (St. Louis, MO, USA). Rhodamine-labeled BSA, penicillin–streptomycin (P/S), trypsin, rhodamine-labeled phalloidin, anti-MHC antibody, and 4′,6-diamidino-2-phenylindole (DAPI) were purchased from Thermo Fisher Scientific (Waltham, MA, USA). *N*-hydroxysuccinimide (NHS)-tethered Cy5 was purchased from Lumiprobe (Hunt Valley, MD, USA). The Mouse Quantikine ELISA kits for VEGF, FGF-2, and HGF were purchased from R&D Systems (Minneapolis, MN, USA). Dialysis membranes (molecular weight cutoff [MWCO] value:12 000–14 000) were purchased from Repligen (MA, USA). Liberase and DNase I were purchased from Merck (Frankfurt, Germany). Dimethyl sulfoxide (DMSO) was purchased from Fujifilm Wako (Osaka, Japan). HA was purchased from Seikagaku Corporation (Tokyo, Japan). HA-fluorescein was purchased from Creative PEG Works (Durham, NC, USA). C57BL/6 mouse bone marrow-derived MSC were purchased from Cyagen (Santa Clara, CA, USA). The MSC growth medium (MesenCult Expansion Medium) was purchased from Veritas (Tokyo, Japan). The C2C12 cell was purchased from the European Collection of Authenticated Cell Cultures.

Synthesis of UPy Units: The UPy units were synthesized as described previously.[45] Briefly, 2-amino-4-hydroxy-6-methylpyrimidine (33.0 mmol, 4.1 g) was dispersed in 1,6-diisocyanatohexane (148.6 mmol, 25.0 g). The reaction was performed at 100 °C for 16 h with stirring. After the mixture was cooled to 25 °C, 10 volumes of *n*-hexane were added to precipitate the product. The precipitate was collected via filtration and washed three times with *n*-hexane. The product was vacuum dried to obtain UPy units with isocyanate groups.

Synthesis of Gelatin Derivatives: Porcine-skin-derived gelatin was used to synthesize gelatin derivatives, including gelatin GUPy, GTH, GVS, GUPyTH, and GUPyVS as previously described.[35–36] Briefly, to synthesize GUPy, gelatin (amino group: 311 µmol g^{-1} in gelatin) was reacted with the UPy units (48% equivalent to the amino groups in gelatin) in DMSO at 6 wt.% at 50 °C under stirring for 24 h. The products were purified by precipitation with 20 volumes of a cold solvent mixture of ethanol and ethyl acetate (v/v = 1/1) and washed with ethanol. The products were vacuum dried to obtain GUPy. The number of amino groups in the gelatin derivatives was measured using TNBS to estimate the degree of substitution (D.S.) of the UPy units, as previously described.[46] The synthesis of GUPy was characterized by ^{1}H-nuclear magnetic resonance (^{1}H NMR, DMSO-d_6, ECZ 400S, 400 MHz, JEOL, Tokyo, Japan). To synthesize GTH and GUPyTH, gelatin and GUPy were reacted with γ-thiobutyrolactone (230 mol% equivalent to the amino groups in gelatin

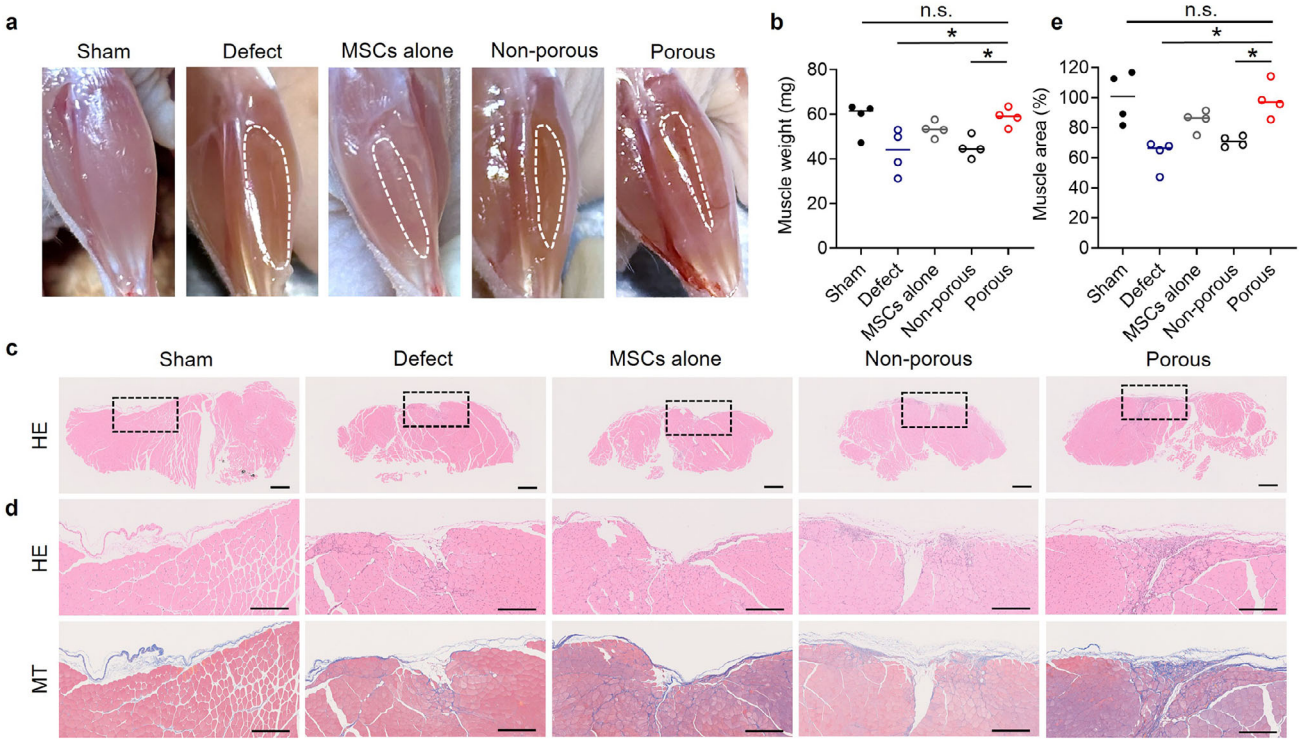

Figure 6. Therapeutic efficacy of porous hydrogels against VML models. a) Gross view of TA muscles of the control, sham, MSCs alone, non-porous and porous hydrogels at 28 days after transplantation. b) Quantification of TA muscle weight after 4 weeks of transplantation ($n = 4$). c) Low magnification cross-sectional HE images of TA muscles. d) High magnification cross-sectional images stained with HE (left) and MT (right). e) TA muscle area estimated from HE images of Figure 6c ($n = 4$). $^{*}p < 0.05$, $^{**}p < 0.01$ analyzed by the one-way ANOVA with Tukey's multiple comparison post hoc test. n.s. denotes not significant. Scale bars represent 500 µm for (c) and 250 µm for (d).

and GUPy) in DMSO at 6 wt.% at 50 °C under stirring for 24 h. After the addition of TCEP-HCl (1 mmol L^{-1}), the products were purified via precipitation with 20 volumes of a cold solvent mixture of ethanol and ethyl acetate (v/v = 1/1) and washed with ethanol. The products were vacuum dried to obtain GTH and GUPyTH. The D.S. of the thiol groups in the gelatin derivatives was calculated using Ellman's method.[47] To synthesize GVS and GUPyVS, GTH (thiol group: 227 µmol g^{-1}) and GUPyTH (thiol group: 138 µmol g^{-1}) were dissolved in ultrapure water (1 wt.%) at 50 °C under stirring. Divinyl sulfone (191 mol%, equivalent to thiol groups in GTH and GUPyTH) was added to the solution. The reaction was performed at 50 °C for 24 h with stirring. After adding TCEP (1 mmol L^{-1}) to the solution, the products were dialyzed in ultrapure water using a dialysis membrane (molecular cutoff: 10 kDa) for 3 days. GVS and GUPyVS were obtained by freeze-drying. The D.S. of the vinyl sulfone groups in the gelatin derivatives was calculated by determining the number of thiol groups in the GVS and GUPyVS.

Synthesis of GTH-fluorescein, GUPy-Cy5, GUPyTH-Cy5.5, and HA-fluorescein: GTH-fluorescein, GUPy-Cy5, GUPy-Cy5, GUPyTH-Cy5.5, and HA-fluorescein were synthesized as previously described. Briefly, GTH was dissolved in DMSO to synthesize GTH-fluorescein, and FITC (1 mol% equivalent to the amino groups in sG) was added to the solution. After precipitation, washing, and drying in the same manner as for the synthesis of GTH, the products were further dialyzed using a dialysis membrane (molecular weight cutoff: 10 kDa) for 3 days. After freeze-drying for 3 days, GTH-fluorescein was obtained. For the synthesis of GUPy-Cy5, gelatin (3 g) was dissolved in DMSO (60 mL) at 50 °C for 2 h and cooled to room temperature. After adding NHS-tethered Cy5 (6.3 mg, 8.8 mol) and UPy units (116 mg, 45%) to the solution, the reaction was continued for 16 h at room temperature. The products were dialyzed using a dialysis membrane (molecular weight cutoff:10 kDa) for 3 days. After freeze-drying for 3 days, GUPy-Cy5 was obtained. GUPyTH-Cy5.5 was synthesized by reacting GUPy-Cy5.5 with thiobutyrolactone in the same manner as described above.

Preparation of Hydrogels: To prepare hydrogels with small and large micropores, GTH (SH groups: 227 µmol) and GVS (VS groups: 223 µmol) were dissolved in PBS at 10 wt.% at 50 °C under stirring. GUPy (D.S. of UPy: 42%) was dissolved in PBS at 10 wt.% for large micropores and 15 wt.% for small micropores at 50 °C under stirring. The pH of each solution was adjusted to 7.4, 6.0, and 7.4 with 1 mol L^{-1} NaOH. The solution was maintained at 37 °C until further use. Solutions of GTH (100 µL), GVS (100 µL), and GUPy (200 µL) were mixed by pipetting up and down 10 times carefully to avoid foaming. The turbid solution was placed on a substrate and incubated for 10 min at 37 °C to obtain hydrogels with small and large micropores. To prepare hydrogels with medium micropores, GUPyTH and GUPyVS were dissolved in PBS at 10 wt.% at 50 °C under stirring. HA was dissolved in PBS at 2 wt.% at 25 °C under stirring. The pH of each solution was maintained at 7.4, 6.0, and 7.4 by using 1 mol L^{-1} NaOH, and the solution was kept at 37 °C until use. Solutions of GUPyTH (100 µL), GUPyVS (100 µL), and HA (100 µL) were mixed in the same way as the mixing method for hydrogels with small and large micropores. The turbid solution was placed on the substrate and incubated at 37 °C for 30 min to obtain hydrogels with medium micropores. To prepare non-porous hydrogels, mixed solutions of GTH (100 µL), GVS (100 µL), and PBS (200 µL) were used.

Confocal Laser Scanning Microscopy (CLSM) Observation: GTH-fluorescein and GUPy-Cy5 were used to visualize LLPS structures. To visualize the small and large hydrogels, the GTH-fluorescein, GVS, and GUPy-Cy5 solutions were mixed using a pipette in a 1:1:2 volume ratio and placed on a coverslip. To visualize the medium-sized hydrogels, GUPyTH-Cy5 and HA-fluorescein solutions were mixed using a pipette at a 1:1:1 volume ratio. Three hydrogels were prepared for each observation. After incubation for 10 min at 37 °C, the samples were observed by CLSM (CLSM 900 with

Airyscan2, Zeiss, Germany). Three CLSM images of each hydrogel type were used to analyze the pore diameter. For pore diameter analysis, 50 points of each hydrogel type were counted from the CLSM images using ImageJ. The overall porosity was quantified by binarizing three CLSM images using ImageJ and IMARIS 10.2 software (Oxford Instruments, UK).

Rheological Measurement: The rheological measurements were performed using a rheometer (MCR301; Anton Paar GmbH, Graz, Austria). Solutions of GTH, GVS, and PBS, or GUPy, were mixed in a 1:1:2 volume ratio at 37 °C to prepare and placed on the stage of the rheometer (pre-warmed to 37 °C) to form GTH+GVS+PBS hydrogels (non-porous hydrogels) and GTH+GVS+GUPy hydrogels (porous hydrogels). A jig with a diameter of 10 mm was placed in the gap of 1 mm. Time-dependent rheological properties were measured at 37 °C at a frequency of 10 rad s^{-1} with a 1% strain in the oscillatory mode.

Swelling Ratio: The swelling ratio of the hydrogels was measured after immersion in PBS at 37 °C. A pre-gel solution (100 µL) of non-porous and porous hydrogels was added to a 2 mL tube. After the gelation at 37 °C for 1 h, PBS (pH = 7.4) was added to each tube and incubated for 24 h at 37 °C. After incubation, the gels were collected and weighed (W_s). The swollen gels were desalted by incubation in water for 1 h, freeze-dried, and weighed (W_d). The swelling ratio was calculated as follows:

$$\text{Swelling ratio} = (W_s - W_d/W_d) \quad (1)$$

where W_s and W_d represent the weight of swelled and dried gels, respectively.

Degradation Test: A pre-gel solution (100 µL) of non-porous and porous hydrogels was added to a 2 mL tube. After gelation at 37 °C for 1 h, PBS (1 mL) with or without 1 mg mL^{-1} of collagenase (120 U mL^{-1}) was added and incubated at 37 °C for 1, 4, 8, and 24 h. After the incubation, the supernatants were discarded, and ultrapure water was added and incubated at 25 °C for 1 h for desalination. The resulting gel was freeze-dried and weighed.

Diffusion Test: A mixture of GTH-fluorescein, GVS, and GUPy-Cy5 solution (20 µL, volume ratio; 1:1:2) was added to an 8 well chamber slide. After incubation for 10 min, PBS (0.3 mL) containing rhodamine-labeled BSA (1 mg mL^{-1}) was added to each dish. After 24 h of incubation, the gels were observed using CLSM.

Encapsulation of Cells in Hydrogel: GTH and GVS were dissolved in PBS at 10 wt.% at 50 °C under stirring. GUPy was dissolved in PBS 20 wt.% at 50 °C under stirring. The pH was adjusted to 7.4, 6.0, and 7.4, using 1 mol L^{-1} NaOH. Solutions of GTH, GVS, and GUPy were filtered with a 0.45 µm filter for sterilization. The solution was maintained at 37 °C until further use. MSCs were cultured in growth medium (MesenCult Expansion Medium). C2C12 cells were cultured in RPMI supplemented with 10% FBS and 1% P/S. Cultured cells were treated with trypsin and collected as pellets after centrifugation at 2500 rpm for 2 min. After removing the supernatant, a mixture of GTH, GVS, and GUPy solution (20 µL, volume ratio: 1:1:2) was added to the pellet of each cell and mixed using a pipette. The 1×10^5 cells were encapsulated in 20 µL of hydrogels for MSCs and C2C12 cells. The mixture was then placed on a chamber cover (10 × 10 mm) and incubated for 30 min at 25 °C for gelation. The medium (400 µL) was added and cultured for 2 d at 37 °C in a 5% CO_2 incubator.

Fluorescence Staining: The cells were then fixed in 4% paraformaldehyde for 1 h. After washing with PBS, the cells were permeabilized with 0.2% Triton-X for 30 min. The cells were treated in a blocking solution (1% BSA/PBS) for 1 h. For actin staining, cells were stained with rhodamine-labeled phalloidin (1:100) overnight at 4 °C. After washing with PBS three times, cells were stained with DAPI for 1 h at 25 °C. For MHC staining, cells were stained with anti-MHC antibody (1:100) for overnight at 4 °C. After washing with PBS for 24 h, cells were stained with goat anti-mouse IgG with Alexa488 as a secondary antibody (1:400) overnight at 4 °C. After washing with PBS for 24 h, cells were stained with DAPI for 1 h at 25 °C. The cellular morphology was observed using CLSM, and the area of the cells was quantified by binarizing three CLSM images using ImageJ software. To quantify the aspect ratio of the cells, cell boundaries were manually traced for each individual cell, and the aspect ratio (major axis to minor axis) was quantified using ImageJ software. Three CLSM images were used for the analysis, and three randomly selected cells were measured from each image.

Cell Proliferation Test: MSCs (6×10^4 cells) were encapsulated in non-porous and porous hydrogels (20 µL) and cultured for 1, 2, and 3 days. After culturing, the hydrogels were degraded using Liberase (0.1 mg mL^{-1}) for 30 min. The cells were collected by centrifugation at 2500 rpm for 2 min, and the number of cells was counted using a hemocytometer on days 0, 1, 2, and 3.

Quantification of VEGF, FGF-2, and HGF Secretion: MSCs (1×10^5 cells) were encapsulated in non-porous and porous hydrogels (20 µL) and cultured for 1 day. Supernatants were collected and used to quantify VEGF, FGF-2, and HGF secretion by ELISA according to the manufacturer's protocol.

Cell Infiltration Test: Non-porous and porous hydrogels (100 µL) were added into a cell culture insert (24 well, 8 µm pore, PET, Corning, USA) to form hydrogels on the permeable membrane. C2C12 cells (1×10^4 cells) were suspended in growth medium (RPMI1640 with 10% FBS and 1% P/S) (100 µL) and seeded onto hydrogels. The medium (2 mL) was added to the insert and the well plate, and the cells were cultured for 4 days. The samples were fixed with 4% paraformaldehyde and stained with rhodamine-labeled phalloidin (1:100). Cellular infiltration was observed using CLSM, and the cell infiltration depth was quantified using IMARIS 10.2 software.

Differentiation Test: C2C12 cells (2×10^5 cells) were encapsulated in non-porous and porous hydrogel (20 µL) and cultured for 3 days in growth medium and 7 days in the differentiation medium (DMEM supplemented with 2% horse serum) at 37 °C and 5% CO_2. C2C12 cells were cultured in a 2D well plate. The samples were stained with an anti-MHC antibody and observed using CLSM, and the myotube length was quantified using ImageJ software.

Biodegradability Test: All the animal experiments were approved by the Animal Care and Use Committee of the National Institute for Materials Science (No.80-2024-01). GTH, GVS, and PBS or GUPy solutions were sterilized by filtration and mixed in a 1:1:2 volume ratio. The pre-gels of non-porous and porous hydrogel were placed in a silicone mold with 1 mm thickness, followed by incubation for 1 h at 25 °C for gelation. The gels formed in the mold were then dissected into 8 mm discs and subcutaneously implanted into the mice. Mice (7-week-old male C57BL/6J mice, Jackson Laboratory, USA) were anesthetized by inhalation of 2% isoflurane. The backs of mice were disinfected with 70% ethanol. The gels were subcutaneously implanted into the backs of mice. At 0, 3, 7, 14, and 28 days after implantation, the mice were euthanized by exsanguination, and tissues were collected. The samples were then fixed in 10% formalin buffer solution for 3 days and sectioned. Images of HE-stained tissues were scanned using a digital slide scanner (NanoZoomer S210, Hamamatsu Photonics, Hamamatsu, Japan). Changes in the hydrogel thickness were quantified using a nanozoomer.

Evaluation of Cell Survival: To prepare the VML models, the TA muscles were injured according to a previous report.[48] Mice (8-week-old male BALB/c-nu, The Jackson Laboratory Japan, Inc.) were anesthetized by inhaling 2% isoflurane. The skin on the lower legs of each mouse was disinfected with 70% ethanol and opened using sterilized scissors and fine forceps. Approximately 20% of the TA muscle was excised from both legs to create volumetrically defective muscles, each measuring $2 \times 5 \times 2$ mm^3. Before injection, mouse MSCs were stained with DiI, according to the manufacturer's protocol. MSCs (2×10^5 cells) were dispersed in 20 µL of PBS or encapsulated in non-porous and porous hydrogels were transplanted into the defects using a pipettor. The skin was closed using a 4-0 suture. The mice were administered intraperitoneally carprofen (5 mg kg^{-1}) for analgesia and antibiotic amikacin (1 mg kg^{-1}). At day 7 after transplantation, tissues were collected, and DiI-labeled transplanted cells were observed by CLSM.

VML Treatment: The VML was created by excising the TA muscle from both legs of the mice (8-week-old male BALB/c-nu), each with a defect size of $2 \times 5 \times 2$ mm^3. Mouse MSCs (2×10^5 cells) were dispersed in 10 µL of PBS and encapsulated in non-porous hydrogel and porous hydrogel were transplanted into the VML defects using a pipettor. Sham and non-treated (defect) groups were used as positive and negative controls,

respectively. The skin was closed using 4-0 suture. The mice were administered carprofen (5 mg kg^{-1}) intraperitoneally for analgesia and antibiotic amikacin (1 mg kg^{-1}). Each group was sacrificed at 4 weeks to evaluate the in vivo recovery of muscle tissue. The obtained TA muscles were weighed and fixed in 10% formalin buffer solution for 3 days, embedded in paraffin, sectioned, and stained with HE and MT. The stained TA muscle was transversely cut at the midpoint, and the cross-sectional area was defined as the muscle area. Tissue images were scanned using a digital slide scanner and analyzed using ImageJ software.

Statistical Analysis: The results are expressed as mean ± SD. ANOVA preliminary conditions were verified using the Shapiro–Wilk test. Two-tailed Student's *t*-test, one-way ANOVA, or two-way ANOVA followed by Tukey's multiple comparison *post hoc* test were conducted for data that followed a normal distribution for differences among the groups. The Mann–Whitney U test or Kruskal–Wallis test, followed by Dunn's multiple comparison test, was used for non-normally distributed data for differences among the groups. Experiments were repeated multiple times as independent experiments. The data shown in each figure is complete dataset obtained from independent representative experiments. None of the samples were excluded from the analysis. Statistical significance is indicated by $^{*}p < 0.05$, $^{**}p < 0.01$, $^{***}p < 0.001$, and $^{****}p < 0.0001$. Statistical analyses were performed using GraphPad Prism software (version 8.0; GraphPad Software).

Supporting Information

Supporting Information is available from the Wiley Online Library or from the author.

Acknowledgements

The authors appreciate the financial support from the Japan Society for the Promotion of Science (JSPS) KAKENHI (grant no. 22H03962), Inamori Foundation, Toshiaki Ogasawara Memorial Foundation, and Uehara Memorial Foundation.

Conflict of Interest

The authors declare no conflict of interest.

Data Availability Statement

The data that support the findings of this study are available from the corresponding author upon reasonable request.

Keywords

cell transplantation, hydrogel, liquid–liquid phase separation, regenerative medicine, volumetric muscle loss

Received: April 2, 2025
Revised: June 3, 2025
Published online:

[1] M. Sandona, L. Di Pietro, F. Esposito, A. Ventura, A. R. Silini, O. Parolini, V. Saccone, *Front Bioeng Biotechnol* **2021**, *9*, 652970.
[2] S. E. Anderson, W. M. Han, V. Srinivasa, M. Mohiuddin, M. A. Ruehle, J. Y. Moon, E. Shin, C. L. San Emeterio, M. E. Ogle, E. A. Botchwey, N. J. Willett, Y. C. Jang, *Tissue Eng., Part C* **2019**, *25*, 59.
[3] C. A. Cezar, D. J. Mooney, *Adv Drug Deliv Rev* **2015**, *84*, 188.
[4] M. A. Machingal, B. T. Corona, T. J. Walters, V. Kesireddy, C. N. Koval, A. Dannahower, W. Zhao, J. J. Yoo, G. J. Christ, *Tissue Eng Part A* **2011**, *17*, 2291.
[5] X. Tang, L. Daneshmandi, G. Awale, L. S. Nair, C. T. Laurencin, *Regen Eng Transl Med* **2019**, *5*, 233.
[6] F. G. Brian, M. A. J. Joseph, *Journal of the AAOS* **2011**, *19*, S35.
[7] B. T. Corona, K. Garg, C. L. Ward, J. S. McDaniel, T. J. Walters, C. R. Rathbone, *Am. J. Physiol. Cell Physiol.* **2013**, *305*, C761.
[8] M. T. Li, N. J. Willett, B. A. Uhrig, R. E. Guldberg, G. L. Warren, *J. Biomech.* **2014**, *47*, 2013.
[9] R. Raman, *Modeling Muscle, Science* **2019**, *363*, 1051.
[10] B. T. Corona, J. C. Rivera, J. C. Wenke, S. M. Greising, *J Exp Orthop* **2017**, *4*, 36.
[11] M. Klinkenberg, S. Fischer, T. Kremer, F. Hernekamp, M. Lehnhardt, A. Daigeler, *Plast. Reconstr. Surg.* **2013**, *131*, 293.
[12] C.-H. Lin, Y.-T. Lin, J.-T. Yeh, C.-T. Chen, *Plast. Reconstr. Surg.* **2007**, *119*, 2118.
[13] H. M. Wobma, D. Liu, G. Vunjak-Novakovic, *ACS Biomater. Sci. Eng.* **2018**, *4*, 1162.
[14] A. Augello, C. De Bari, *Hum. Gene Ther.* **2010**, *21*, 1226.
[15] G. Yang, X. Fan, Y. Liu, P. Jie, M. Mazhar, Y. Liu, N. Dechsupa, L. Wang, *Stem Cell Rev. Rep.* **2023**, *19*, 1214.
[16] R. Lev, D. Seliktar, *J R Soc Interface* **2018**, *15*, 20170380.
[17] C. Fuoco, L. L. Petrilli, S. Cannata, C. Gargioli, *J Orthop Surg Res* **2016**, *11*, 86.
[18] M. Ghanbari, M. Salavati-Niasari, F. Mohandes, Z. Firouzi, S.-D. Mousavi, *J. Mol. Liq.* **2021**, *335*, 116531.
[19] Z. Wang, Z. Lin, X. Mei, L. Cai, K. C. Lin, J. F. Rodriguez, Z. Ye, X. S. Parraguez, E. M. Guajardo, P. C. Garcia Luna, J. Y. J. Zhang, Y. S. Zhang, *Adv. Mater.* **2025**, *37*, 2416260.
[20] P. Genovese, A. Patel, N. Ziemkiewicz, A. Paoli, J. Bruns, N. Case, S. P. Zustiak, K. Garg, *J Tissue Eng Regen Med* **2021**, *15*, 1131.
[21] N. Matthias, S. D. Hunt, J. Wu, J. Lo, L. A. Smith Callahan, Y. Li, J. Huard, R. Darabi, *Stem Cell Res.* **2018**, *27*, 65.
[22] N. G. Kozan, M. Joshi, S. T. Sicherer, J. M. Grasman, *Front Bioeng Biotechnol* **2023**, *11*, 1245897.
[23] A. Rossi, G. Bassi, C. Cunha, C. Baldisserri, N. Ravaglia, D. Gardini, F. Molinari, F. Lista, F. J. Teran, A. Piperno, M. Montesi, S. Panseri, *J. Colloid Interface Sci.* **2025**, *678*, 334.
[24] N. Ueda, S. Sawada, F. Yuasa, K. Kato, K. Nagahama, *ACS Appl. Mater. Interfaces* **2022**, *14*, 52618.
[25] L. A. Bosworth, S. R. Rathbone, R. S. Bradley, S. H. Cartmell, *J. Mech. Behav. Biomed. Mater.* **2014**, *39*, 175.
[26] R. D. Cardwell, L. A. Dahlgren, A. S. Goldstein, *J Tissue Eng Regen Med* **2014**, *8*, 937.
[27] J. Gilbert-Honick, S. R. Iyer, S. M. Somers, R. M. Lovering, K. Wagner, H.-Q. Mao, W. L. Grayson, *Biomaterials* **2018**, *164*, 70.
[28] M. Ghanbari, M. Salavati-Niasari, F. Mohandes, *Int. J. Pharm.* **2021**, *602*, 120660.
[29] F. J. O'Brien, B. A. Harley, I. V. Yannas, L. J. Gibson, *Biomaterials* **2005**, *26*, 433.
[30] W. Kim, H. Hwangbo, G. Heo, D. Ryu, G. Kim, *Adv. Funct. Mater.* **2024**, *35*, 2406591.
[31] N. Huebsch, E. Lippens, K. Lee, M. Mehta, S. T. Koshy, M. C. Darnell, R. M. Desai, C. M. Madl, M. Xu, X. Zhao, O. Chaudhuri, C. Verbeke, W. S. Kim, K. Alim, A. Mammoto, D. E. Ingber, G. N. Duda, D. J. Mooney, *Nat. Mater.* **2015**, *14*, 1269.
[32] X. Yang, B. Yang, Y. Deng, X. Xie, Y. Qi, G. Yan, X. Peng, P. Zhao, L. Bian, *Adv. Mater.* **2023**, *35*, 2300636.
[33] J. Koh, D. R. Griffin, M. M. Archang, A. C. Feng, T. Horn, M. Margolis, D. Zalazar, T. Segura, P. O. Scumpia, D. Di Carlo, *Small* **2019**, *15*, 1903147.

[34] E. Sleep, B. D. Cosgrove, M. T. McClendon, A. T. Preslar, C. H. Chen, M. H. Sangji, C. M. R. Pérez, R. D. Haynes, T. J. Meade, H. M. Blau, S. I. Stupp, *Proc Natl Acad Sci U S A* **2017**, *114*, E7919.
[35] A. Nishiguchi, E. Araki, D. Palai, S. Ito, T. Taguchi, *Biomacromolecules* **2024**, *25*, 6146.
[36] A. Nishiguchi, S. Ito, K. Nagasaka, H. Komatsu, K. Uto, T. Taguchi, *Biomaterials* **2024**, *305*, 122451.
[37] O. Y. Dudaryeva, L. Cousin, L. Krajnovic, G. Gröbli, V. Sapkota, L. Ritter, D. Deshmukh, Y. Cui, R. W. Style, R. Levato, C. Labouesse, M. W. Tibbitt, *Adv. Mater.* **2025**, *37*, 2410452.
[38] T. H. Qazi, D. J. Mooney, G. N. Duda, S. Geissler, *Biomaterials* **2017**, *140*, 103.
[39] N. Ferrara, *Endocr Rev* **2004**, *25*, 581.
[40] U. G. Longo, M. Loppini, A. Berton, F. Spiezia, N. Maffulli, V. Denaro, *Stem Cells Int* **2012**, *2012*, 175038.
[41] S. M. Sheehan, R. E. Allen, *J. Cell. Physiol.* **1999**, *181*, 499.
[42] M. C. Lee, J. S. Lee, S. Kim, A. Jamaiyar, W. Wu, M. L. Gonzalez, T. C. A. Durán, A. D. Madrigal-Salazar, N. Bassous, V. Carvalho, C. Choi, D.-S. Kim, J. W. Seo, N. Rodrigues, S. F. C. F. Teixeira, A. F. Alkhateeb, J. A. L. Soto, M. A. Hussain, J. Leijten, M. W. Feinberg, S. R. Shin, *Adv. Mater.* **2025**, *37*, 2408488.
[43] S. Ostrovidov, V. Hosseini, S. Ahadian, T. Fujie, S. P. Parthiban, M. Ramalingam, H. Bae, H. Kaji, A. Khademhosseini, *Tissue Eng Part B Rev* **2014**, *20*, 403.
[44] G. C. Gurtner, S. Werner, Y. Barrandon, M. T. Longaker, *Nature* **2008**, *453*, 314.
[45] B. J. B. Folmer, R. P. Sijbesma, R. M. Versteegen, J. A. J. Rijt, E. W. Meijer, *Adv. Mater.* **2000**, *12*, 874.
[46] H. H. Zhao, N. D. Heindel, *Pharm. Res.* **1991**, *08*, 400.
[47] D. S. B. Dennis, R. Jenke, *Anal. Chem.* **1987**, *59*, 1509.
[48] I. Eugenis, D. Wu, C. Hu, G. Chiang, N. F. Huang, T. A. Rando, *Biomaterials* **2022**, *290*, 121818.